Autoresonances of $m = 2$ diocotron oscillations in non-neutral electron plasmas

K. Gomberoff,[1] H. Higaki,[2] C. Kaga,[2] K. Ito,[2] and H. Okamoto[2]
[1]*Zalman Shazar 6/25, Kiryat Motzkin, Haifa 2623024, Israel*
[2]*Graduate School of Advanced Sciences of Matter, Hiroshima University, 1-3-1 Kagamiyama, Higashi-Hiroshima, Hiroshima 739-8530, Japan*
(Received 1 March 2016; published 24 October 2016)

The existence of autoresonances for $m = 2$ diocotron oscillations of non-neutral electron plasmas in a uniform magnetic field was predicted by particle-in-cell simulations and it was confirmed in experiments. The obtained results show clear deviations from the standard threshold amplitude dependence on the sweep rate. The threshold amplitude approaches a constant at a lower sweep rate when there is a damping force. It was also found that the aspect ratio for the oval cross section of the confined plasma can be controlled by the frequency of the externally applied driving force.

DOI: 10.1103/PhysRevE.94.043204

I. INTRODUCTION

Autoresonance is a phenomenon observed in a wide range of nonlinear oscillations. Thus, autoresonances have been studied in various fields, i.e., atomic physics, plasma physics, solid state physics, and so on [1–8]. Unique features of autoresonance are that the oscillation frequency of the system follows that of the external driving force when the driving amplitude exceeds a threshold amplitude and that it becomes possible to control the amplitude of the oscillation by the driving frequency.

When a single particle of mass m is confined in a one-dimensional potential $U(x) = -U_0 \cos x$, a solution for the equation of motion $\ddot{x} + \omega_0^2 \sin x = 0$ ($\omega_0^2 \equiv U_0/m$) can be expressed with Jacobi's elliptic functions. Here $f_0 = \omega_0/2\pi$ is the small-amplitude resonance frequency. With an additional driving force $F = F_0 \cos(\omega_0 t - \alpha t^2/2)$, the equation of motion becomes

$$\ddot{x} + \omega_0^2 \sin x = \epsilon \cos(\omega_0 t - \alpha t^2/2) \quad (\epsilon \equiv F_0/m), \tag{1}$$

where the driving frequency f $(= f_0 - \alpha t/2\pi)$ changes linearly as a function of time t and α is defined as a sweep rate.

In the case of non-neutral plasmas, $m = 1$ diocotron oscillations [9–12] and Bernstein-Greene-Kruskal modes [13] have been studied. The autoresonance for the axial harmonic oscillation of an antiproton plasma has been applied for the production of antihydrogen atoms [14,15]. The obtained results were well explained by a theoretical model [16,17], which revealed that the threshold amplitude V_{th} is proportional to the power of the sweep rate as

$$V_{th} \propto \alpha^{3/4}. \tag{2}$$

Hereafter, this dependence is referred to as the standard threshold amplitude dependence.

So far, there are several reports on the autoresonance with a damping term $m\gamma\dot{x}$ [6,7,11,12], whose equation of motion is given by

$$\ddot{x} + \gamma\dot{x} + \omega_0^2 \sin x = \epsilon \cos(\omega_0 t - \alpha t^2/2). \tag{3}$$

In a superconducting Josephson resonator, it was observed that $V_{th}(\alpha)$ deviated slightly from the standard one [6] and the effect of the Q $(= \omega_0/\gamma)$ factor on $m = 1$ diocotron oscillations was reported [11]. Also, numerical calculations for Eq. (3) suggest that $V_{th}(\alpha)$ can deviate significantly from the standard one at smaller α [18].

In this paper we report simulation and experimental results on the autoresonances for $m = 2$ diocotron oscillations of non-neutral electron plasmas in a uniform magnetic field, which is an example of autoresonance with a damping term. Being different from autoresonances of the $m = 1$ diocotron oscillation and axial harmonic oscillation, in which the center of mass moves as an oscillator, the center of mass stays on the axis of symmetry for $m = 2$ diocotron oscillations. Instead, the cross section of the oval profile changes as a function of resonant frequency [19] and the decay constant of the oscillation becomes much larger. Experimental results on the $m = 1$ diocotron oscillation and axial harmonic oscillation are also presented for a comparison of the damping terms.

II. SETUP FOR EXPERIMENTS AND SIMULATIONS

A. Experimental setup

A schematic of the experimental setup for $m = 2$ diocotron oscillations is shown in Fig. 1(a). Non-neutral electron plasmas are confined with a multiring electrode trap, which contains 45 ring electrodes with an inner radius of $R = 35$ mm and an axial length of 12 mm. There are 4-mm gaps between electrodes. Five electrodes denoted by closed squares are segmented azimuthally into four pieces, so azimuthal oscillations can be excited and detected. The radial and axial confinement is provided by a uniform magnetic field of ∼96 G and the electrostatic potential $V_1 = V_2 = -50$ V that is applied to five electrodes at both ends. Thus, the axial length of the confined electron plasma becomes ∼57 cm. Other electrodes are grounded except two sets of azimuthally segmented electrodes. For $m = 2$ diocotron experiments, a pair of azimuthally segmented electrodes at the center is connected to an oscillator and another pair of azimuthally segmented electrodes at the different axial position is used to pick up signals through an amplifier, as shown in the figure. For $m = 1$ diocotron experiments, the pairs of segmented electrodes are disconnected.

The experimental procedure is as follows. At first, electrons from a cathode are injected for 1 s by reducing the potential

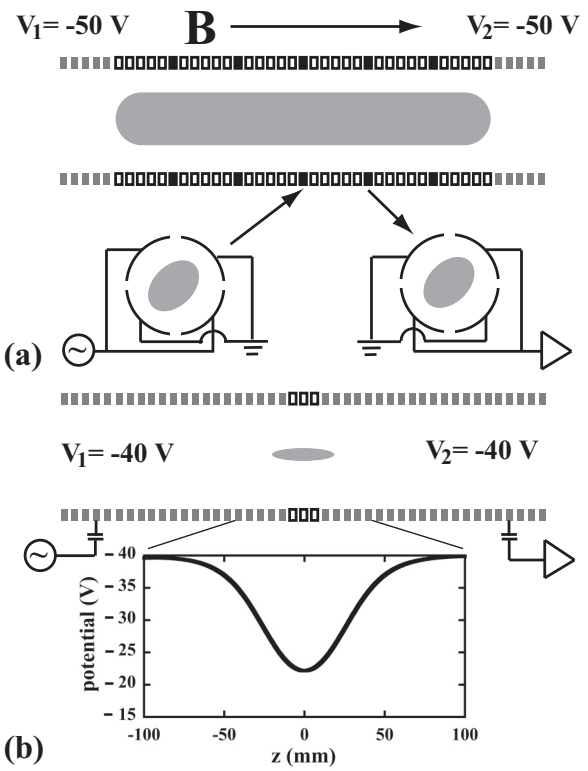

FIG. 1. (a) Schematic drawing of the experimental setup for $m = 1$ and 2 diocotron autoresonances of non-neutral electron plasmas in a uniform magnetic field $B \sim 96$ G. Open squares are grounded ring electrodes. Five pairs of solid squares represent azimuthally segmented electrodes. Gray squares at both ends are ring electrodes where the potentials V_1 and V_2 are applied. The number of electrons is changed by the cathode potential and V_1 during the electron injection. (b) Experimental setup for autoresonances of the axial harmonic oscillations $B \sim 190$ G.

V_1. Typically, $(6.5–9.5) \times 10^8$ electrons are confined with a density of $\sim 10^6\,\mathrm{cm}^{-3}$. The number of electrons is changed to control the density of the plasma and f_0 for the $m = 2$ diocotron oscillations. After a holding time of ~300 ms, an external rf drive is applied for a few milliseconds with a fixed sweep rate and the excited signal is recorded simultaneously with a digital oscilloscope. To detect the number of electrons the potential V_2 is grounded to guide electrons towards a Faraday cup, which is made of a phosphor screen coated with an Al foil with a thickness of ~500 Å. A CCD camera behind the phosphor screen is used to record the images of the extracted electron plasmas when necessary.

Also shown in Fig. 1(b) is the experimental setup for autoresonances of axial harmonic oscillations with a uniform magnetic field of ~190 G. In this case, only a part of the trap is used for the confinement of electrons. Three electrodes at the center and other electrodes are biased to −15 and −40 V, respectively. The potential created on the axis of symmetry is shown by the solid line in the figure. The small-amplitude axial oscillation frequency in this case is $f_0 \sim 9.5$ MHz. The experimental procedure is almost the same, but the electrons are injected only for 400 μs, which results in an electron number of $\sim 1.9 \times 10^7$. The holding time is made 5 s to make sure that all the electrons are at the bottom of the potential through collisions with background neutrals. Then an external driving force is applied to ring electrodes for a few milliseconds with a fixed sweep rate and the excited signal is detected from electrodes on the other side.

B. WARP simulations

Originally, the autoresonances for $m = 2$ diocotron oscillations were found with the particle-in-cell (PIC) code WARP [20,21], which has been a powerful tool to predict and study several non-neutral plasma experiments and phenomena [22–25]. Here WARP simulations are applied to evaluate autoresonances of $m = 2$ diocotron oscillations for the current experimental setup. One of the advantages of using WARP is its capability of calculating the proper particle drifts and Lamor radius without resolving the gyromotion in space and time. The time step is 10^{-8} s and the grid sizes are 2 mm along the magnetic field and 0.9 mm in the perpendicular plane to the magnetic field. Most of the simulation geometries, i.e., the magnetic field, radius of electrodes, plasma length, and so on, are the same with experiments.

However, it should be noted that the experimental conditions are not perfectly reproduced in the simulations. In general, PIC simulations do not include a realistic model for collisions and collisions exist only artificially via numerical effects. In fact, the growth rates of the modes and their decay constants in simulations are faster than those in the experiments. Also, the plasma density cannot be too high, because the grid space should be less than the Debye length. The smaller grid space results in the unfavorably longer calculation time. Furthermore, the required long calculation time makes it difficult to evaluate threshold amplitudes in smaller α. In consequence, the resonance frequency can be different from the one in experiment. This is compensated for with the use of the normalized sweep rate $\alpha_n \equiv \alpha/2\pi f_0^2$, which means how much the frequency is swept during one cycle of the small-amplitude resonance frequency f_0. The normalized sweep rate is useful to compare experimental results with calculations that have different f_0.

In simulations, electrons are not injected but prepared inside the trap from the beginning. The initial circular radial density profile measured in an experiment is imitated and an ideal local equilibrium with cylindrical symmetry is calculated by assuming the Boltzmann distribution at a constant radius and solving the Poisson equation [20]. Then an external rf drive is applied to observe if an autoresonance is excited or not.

In spite of these limitations, the correspondence of radial profiles of plasmas between experiments and simulations are good, which ensures the feasibility of WARP for the current investigation. Shown in Fig. 2 are examples of the radial profiles of a plasma when the $m = 2$ diocotron oscillation is excited with large-amplitude rf bursts.

III. RESULTS AND DISCUSSION

A. Threshold amplitudes

Shown in Fig. 3 are the experimental results for $m = 2$ diocotron oscillations with $f_0 \sim 240$ kHz. In Figs. 3(a) and 3(b), the external drive is applied for 4 ms (from time 0

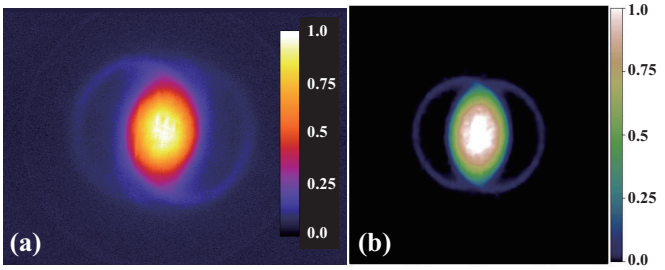

FIG. 2. Radial profiles of a plasma with a large amplitude $m = 2$ diocotron oscillation observed in (a) an experiment and (b) a simulation. The circular halo around the oval core is created when the $m = 2$ diocotron oscillation is excited with large-amplitude rf bursts.

to 4 ms) by sweeping the frequency from 240 to 232 kHz, which corresponds to $\alpha/2\pi = 2$ kHz/ms. The excited signal is recorded for 10 ms (10 Ms/s, 100 kpts) and a fast Fourier transformation (FFT) is applied 100 times for 10 kpts (1 ms) by shifting 1 kpts (0.1 ms) every time to observe the time variation of the excited signal. When the amplitude of the external drive V_d is 1.0 V, which is below a threshold, the frequency of the excited signal stays almost constant around 240 kHz, as in Fig. 3(a). Here the darker tone means the lower power and the white line reflects the frequency of the excited oscillation. On the other hand, when V_d becomes 1.1 V, which is above a threshold, it can be clearly seen in Fig. 3(b) that the frequency of the excited oscillation follows that of the external drive, which is used to judge if the external drive results in autoresonance or not. It can also be seen that the frequency of the excited oscillation goes back to the original frequency after the external drive is stopped at 4 ms.

The measurement is repeated by changing the sweep rate and driving amplitude to obtain the threshold amplitude V_{th} as a function of sweep rate $\alpha/2\pi$, which is plotted in Fig. 3(c). The upper horizontal axis is α_n. The error bars in the figure correspond to the voltage step ΔV used to scan the external rf amplitude. Although there are shot by shot fluctuations, $\pm\Delta V$ covers the fluctuations. It can be clearly seen that the V_{th} dependence deviates from the standard dependence of $\alpha^{3/4}$ at the smaller α. The dotted line is the fitting curve $V_{th} = (0.81 \pm 0.12) + (0.17 \pm 0.05)\alpha^{0.78\pm0.06}$. This means that there is a critical amplitude of 0.81 ± 0.12 V for the onset of autoresonance, below which the external drive is no longer sufficient to overcome the damping losses. In fact, this is consistent with the prediction of the theoretical model [11]. Following the theoretical models in Refs. [11,17], the threshold of the normalized drive strength with a damping term can be expressed by

$$\epsilon_{th} = \sqrt{\frac{8}{\omega_0}}\left\{\left(\frac{\alpha}{3} + \frac{\gamma^2}{16}\right)^{1/2} + \frac{\gamma}{4}\right\}^{3/2}$$
$$= \frac{2f_0}{\sqrt{\pi}}\left\{\left(\frac{2\pi}{3}\alpha_n + \frac{\gamma_n^2}{16}\right)^{1/2} + \frac{\gamma_n}{4}\right\}^{3/2}, \qquad (4)$$

where $\gamma_n \equiv \gamma/f_0$ is the normalized decay constant. This means that ϵ_{th} approaches constant when α becomes negligible to γ^2. When α dominates the damping term, the original result ($\propto\alpha^{3/4}$) is reproduced. The fitting curve with Eq. (4) overlaps the one shown in Fig. 3(c), which gives $\gamma_n = 0.032 \pm 0.002$.

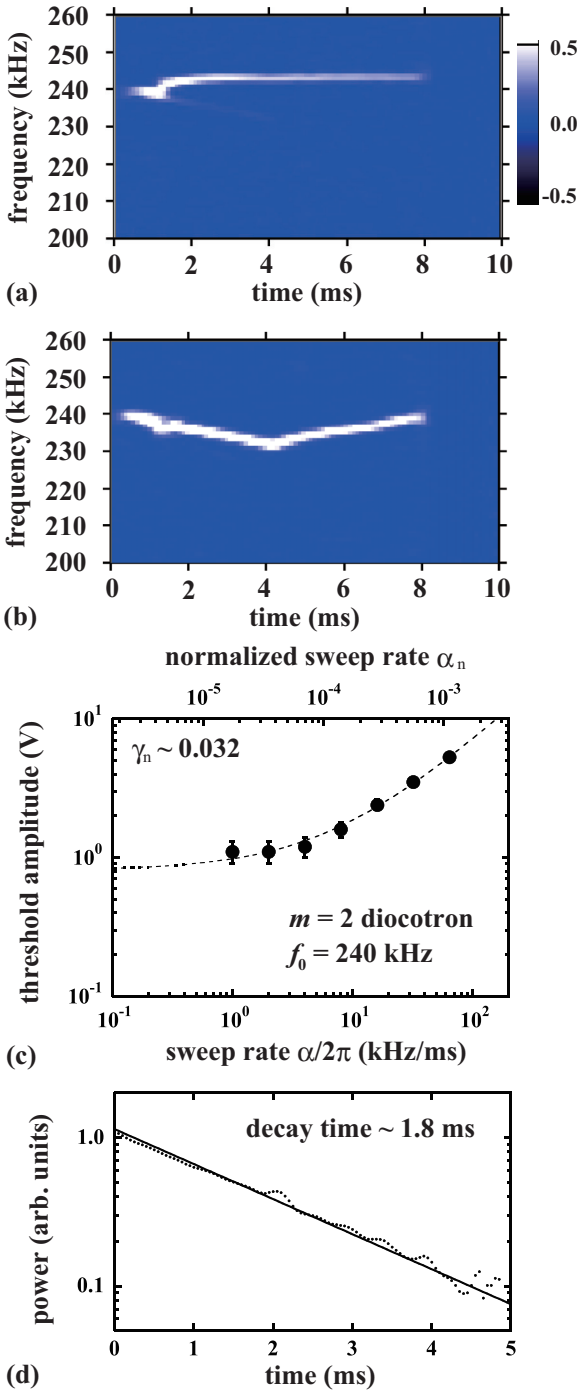

FIG. 3. Autoresonance for $m = 2$ diocotron oscillation with $f_0 \sim 240$ kHz. (a) FFT spectra below a threshold amplitude V_{th}. The frequency of the excited oscillation stays constant. (b) FFT spectra above V_{th}. The frequency of the excited oscillation follows that of the external drive. (c) V_{th} as a function of $\alpha/2\pi$. It deviates from the standard dependence of $\alpha^{3/4}$ at the lower sweep rate. (d) The decay time constant of the small amplitude $m = 2$ diocotron oscillation is about 1.8 ms, which corresponds to the normalized decay constant $\gamma_n \sim 0.0023$.

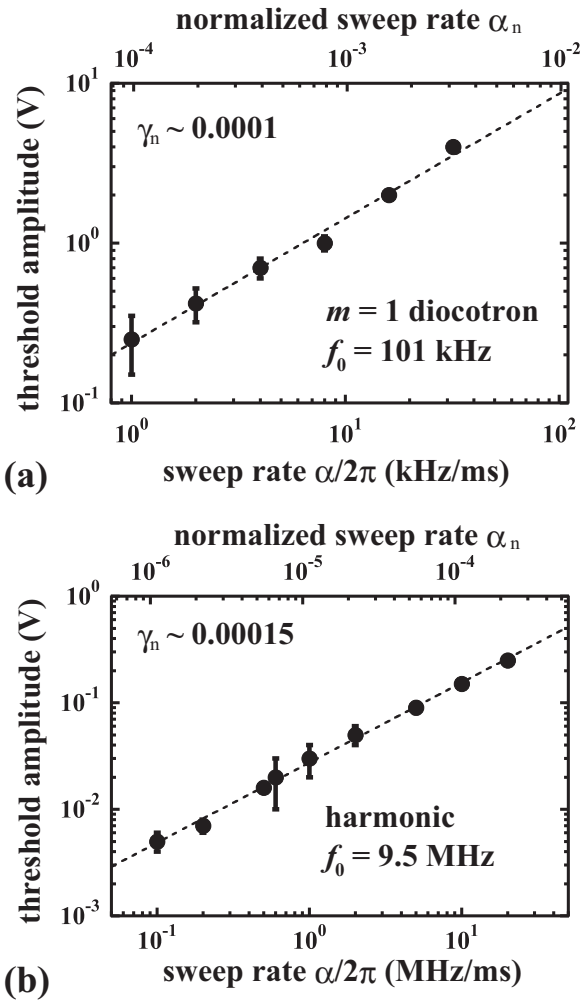

FIG. 4. (a) Threshold amplitude dependence on the sweep rate for $m = 1$ diocotron autoresonances. (b) Threshold amplitude dependence on the sweep rate for autoresonances of the axial harmonic oscillations.

Diocotron oscillations excited in non-neutral electron plasmas have natural decay time constants. The dotted line in Fig. 3(d) shows an example of the measurement for a small amplitude $m = 2$ diocotron oscillation with $f_0 \sim 240$ kHz. The oscillation is excited by rf bursts just before 0 ms and the power of the excited signal is plotted as a function of time. The exponential fitting (solid line) gives a decay time constant of ~1.8 ms, which corresponds to $\gamma_n \sim 0.0023$. It should be noted that this decay constant is obtained after a small-amplitude burst, which is probably different from the one obtained with a large-amplitude external drive.

For comparison with the results obtained for $m = 2$ diocotron oscillations, a similar measurement is performed for autoresonances of the $m = 1$ diocotron oscillation with $f_0 \sim$ 101 kHz and an axial harmonic oscillation with $f_0 \sim 9.5$ MHz. The obtained threshold amplitudes are plotted as functions of $\alpha/2\pi$ in Fig. 4. For the $m = 1$ diocotron oscillation in Fig. 4(a), the fitting line is proportional to $\alpha^{0.78\pm0.09}$ and the observed normalized decay constant is $\gamma_n \sim 0.0001$, which is about 20 times smaller than that of the $m = 2$ diocotron

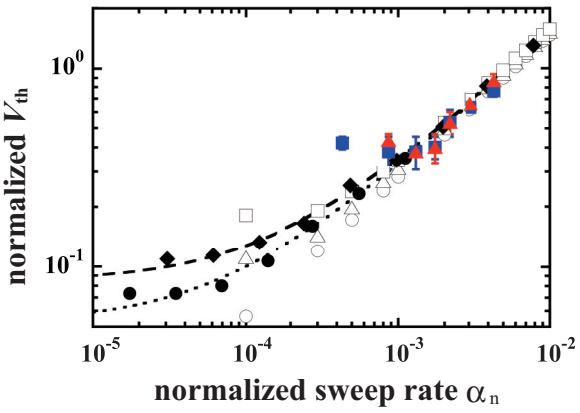

FIG. 5. Red triangles and blue squares are V_{th} determined by WARP simulations with different numbers of macroparticles. Open circles, triangles, and squares are V_{th} obtained from calculations with $\gamma_n = 2\pi \times 0.001$, $2\pi \times 0.003$, and $2\pi \times 0.005$, respectively [18]. Solid circles and diamonds are the normalized experimental data for $f_0 \sim 240$ and 404 kHz, respectively. Dotted and dashed lines are the fitting curves with Eq. (4), which gives $\gamma_n \sim 0.032$ and 0.045 for $f_0 \sim 240$ and 404 kHz, respectively.

oscillation. Also, for the harmonic oscillation in Fig. 4(b), there is no clear deviation from the standard dependence. The fitting line is $\alpha^{0.75\pm0.01}$ and γ_n is 0.000 15, which is also much smaller than that of the $m = 2$ diocotron oscillation. The smaller decay constants of the $m = 1$ diocotron oscillation and the axial harmonic oscillation mean weaker damping than that of the $m = 2$ diocotron oscillation. The comparison with α_n between Figs. 3(c) and 4(b) makes it clear that the threshold amplitude approaches a constant at a lower sweep rate when there is a damping force. In fact, the power fitting with the data $\alpha_n \geqslant 10^{-4}$ in Fig. 3(c) gives a threshold dependence of $V_{th} \propto \alpha_n^{0.57\pm0.03}$, which also deviates clearly from that of the $m = 1$ diocotron oscillation in Fig. 4(a).

In Fig. 5 the experimental results for $m = 2$ diocotron oscillations with $f_0 \sim 240$ kHz (closed circles) and $f_0 \sim$ 404 kHz (closed diamonds) are plotted with numerical calculations for the equation of motion below, where the normalized time is $t_n = tf_0$:

$$\ddot{x} + \gamma_n \dot{x} + 4\pi^2 \sin x = \frac{\epsilon}{f_0^2} \cos\left[2\pi\left(t_n - \alpha_n t_n^2/2\right)\right]. \quad (5)$$

Open circles, triangles, and squares correspond to the threshold amplitudes calculated with $\gamma_n = 2\pi \times 0.001, 2\pi \times 0.003$, and $2\pi \times 0.005$ [18]. Although the sweep rate can be normalized with α_n, it is difficult to normalize the threshold amplitude. This is because the threshold amplitude obtained in experiment is the output voltage of the oscillator, which is different from the amplitude applied to electron plasmas with different parameters. Here the experimental threshold amplitudes are normalized to the calculated value at $\alpha_n = 10^{-3}$. Dotted and dashed lines are the fitting curves for experiments with Eq. (4), which gives $\gamma_n = 0.032 \pm 0.002$ for $f_0 \sim 240$ kHz and $\gamma_n = 0.045 \pm 0.002$ for $f_0 \sim 404$ kHz. These values are 10 times larger than those for the small-amplitude oscillation. It is thought that the difference is due to the nonlinearity of the oscillations with the driving force, which results in the

deformation of the plasma cross section with a velocity shear and viscosity. In fact, it can be said that γ_n in the nonlinear regime with the driving force is measured through the present experiments.

The deviation from the standard threshold amplitude dependence is also observed in simulations. Due to the long calculation time necessary, the smallest $\alpha/2\pi$ in simulations is limited to 25 kHz/ms, which corresponds to $\alpha_n \sim 4 \times 10^{-4}$. Red triangles and blue squares in Fig. 5 are V_{th} obtained by WARP simulations with macroparticles of 5×10^5 and 2.5×10^5 for $\sim 2.8 \times 10^8$ electrons, respectively. It can be seen in Fig. 5 that the simulation results deviate from the standard threshold amplitude dependence at larger α_n compared with experiments. In general, fewer macroparticles with the higher weight lead to the higher numerical collisions. It is thought that the numerical collisions result in the higher damping rate compared with experiments. Nevertheless, it can be seen that the deviations of V_{th} from the standard dependence at the smaller α_n in simulations are reproduced.

B. Oval cross section of a plasma

In Ref. [19] the frequency of a large-amplitude $m = 2$ diocotron oscillation without applied fields was obtained as a function of the aspect ratio λ as in Eq. (6), where a plasma column is characterized by a constant density n, an ellipsoidal cross section with the constant area A_p, and its aspect ratio λ. Here c and e are the speed of light and electron charge, respectively. Five lines in Fig. 6(a) are the normalized $m = 2$ diocotron frequency as a function of λ calculated with Eq. (6) for different values of $\sqrt{A_p/\pi R^2} \equiv r_p/R$,

$$2\pi f = \frac{2cen\pi}{B}\left[\frac{2\lambda}{(1+\lambda)^2} + \frac{A_p^2}{4\pi^2 R^4}\frac{1+\lambda^2}{\lambda}\right] \tag{6}$$

$$\sim \frac{\omega_D}{2}\left[1 + \left(\frac{r_p^2}{R^2}\right)^2 - \frac{(\Delta\lambda)^2}{4}\left\{1 - 2\left(\frac{r_p^2}{R^2}\right)^2\right\}\right]. \tag{7}$$

Introducing the effective circular plasma radius r_p and expanding Eq. (6) with $\lambda = 1 + \Delta\lambda$ up to the second order in $\Delta\lambda$, Eq. (6) can be approximated as Eq. (7), where the diocotron frequency is denoted by $\omega_D \equiv 2cen\pi/B$. When $r_p/R < 2^{-1/4} \sim 0.84$, the $m = 2$ diocotron frequency becomes smaller as λ (or $\Delta\lambda$) becomes larger. The fact that the frequency in Eq. (7) is proportional to $1 - c_0(\Delta\lambda)^2$ (c_0 is a constant) means that x in Eq. (5) can be replaced with $\Delta\lambda$ in the case of the $m = 2$ diocotron oscillation. Thus, in autoresonances of $m = 2$ diocotron oscillations, it is expected that an elliptical cross section of the plasma (i.e., λ) can be controlled with the applied frequency.

The closed circles in Fig. 6(a) are experimental data. In experiments, it was confirmed that the smaller stop frequency results in the larger λ. Images in Figs. 6(b)–6(e) are obtained with $\alpha = 5$ kHz/ms and $V_d = 2.0$ V for the case of $m = 2$ diocotron oscillations with $f_0 \sim 240$ kHz. Only the sweep time is changed to obtain images at the end of the external drive with the different stop frequencies of 230, 220, 210, and 200 kHz for Figs. 6(b), 6(c), 6(d), and 6(e), respectively. It can be seen from the images that some electrons are lost and the area of

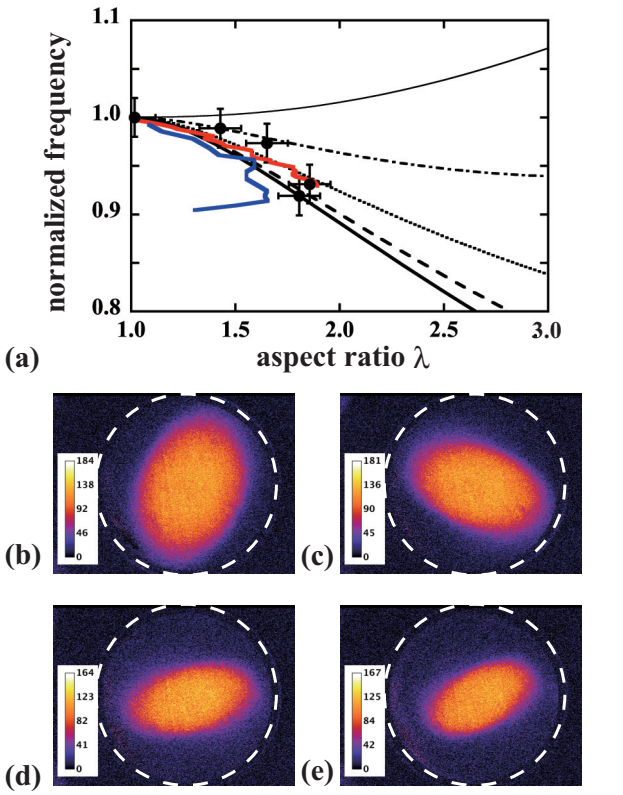

FIG. 6. (a) Normalized frequency of $m = 2$ diocotron oscillations as a function of the aspect ratio λ calculated with Eq. (6). The thick solid line, dashed line, dotted line, dash-dotted line, and thin line correspond to $\sqrt{A_p/\pi R^2} \sim 0.29$, 0.43, 0.57, 0.71, and 0.86, in Eq. (6), respectively. Closed circles are from experiments and the red and blue lines are the simulation results. Also shown are phosphor screen images of plasmas extracted at the end of the external drive for the different stop frequencies of (b) 230, (c) 220, (d) 210, and (e) 200 kHz, respectively.

the plasma cross section becomes smaller, when λ becomes larger. This means that the resonance frequency without the external drive becomes smaller due to the smaller r_p. It was also confirmed by keeping the plasma after the external drive was stopped that the resonance frequency goes back to a final frequency $f_{\rm fin}$, which is less than the original $f_0 \sim 240$ kHz. The solid circles are the stop frequency normalized by the final frequency $f_{\rm fin}$ as a function of λ.

The fact that the cross section of a plasma changes as a function of the drive frequency is also confirmed in WARP simulations. The red and blue lines in Fig. 6(a) are obtained in WARP simulations, which agree with Eq. (6). In the case of the blue line, as the λ becomes too high with a strong nonlinearity, the autoresonance is lost and the cross section of a plasma goes back to a circular one. A similar behavior is also observed in experiments.

In general, the resonance frequency of the nonlinear oscillation depends on its amplitude. Examples are the $m = 1$ diocotron oscillation and the axial harmonic oscillation of non-neutral plasmas in a uniform magnetic field. In addition, autoresonance makes it possible to control the oscillation amplitude through the external driving frequency. The obtained results on $m = 2$ diocotron oscillations suggest that if the

nonlinear resonance frequency depends on another parameter, the external driving frequency can control the parameter through autoresonance.

IV. SUMMARY

Autoresonances of $m = 2$ diocotron oscillations in non-neutral electron plasmas in a uniform magnetic field were investigated in both particle simulations and experiments. A unique feature in this case is that the dependence of the threshold amplitude V_{th} on the sweep rate α deviated from that of the standard autoresonance $V_{th} \propto \alpha^{3/4}$. The results of experiments and simulations showed that the damping force imposed a stricter condition for the onset of autoresonance. The threshold amplitude approached a constant at the lower sweep rate when there was a damping force, which was consistent with the prediction of the theoretical model [11]. Also, it was found that an elliptical cross section of the plasma (i.e., the aspect ratio) could be controlled with the applied frequency.

ACKNOWLEDGMENT

This work was partly supported by JSPS KAKENHI Grant No. 24340142.

[1] B. Meerson and L. Friedland, Phys. Rev. A **41**, 5233 (1990).
[2] L. Friedland, Phys. Fluids B **4**, 3199 (1992).
[3] L. Friedland, Phys. Plasmas **1**, 421 (1994).
[4] L. Friedland, Phys. Rev. E **58**, 3865 (1998).
[5] E. Grosfeld and L. Friedland, Phys. Rev. E **65**, 046230 (2002).
[6] O. Naaman, J. Aumentado, L. Friedland, J. S. Wurtele, and I. Siddiqi, Phys. Rev. Lett. **101**, 117005 (2008).
[7] I. Barth, L. Friedland, E. Sarid, and A. G. Shagalov, Phys. Rev. Lett. **103**, 155001 (2009).
[8] I. Barth, L. Friedland, O. Gat, and A. G. Shagalov, Phys. Rev. A **84**, 013837 (2011).
[9] J. Fajans, E. Gilson, and L. Friedland, Phys. Rev. Lett. **82**, 4444 (1999).
[10] J. Fajans, E. Gilson, and L. Friedland, Phys. Rev. E **62**, 4131 (2000).
[11] J. Fajans, E. Gilson, and L. Friedland, Phys. Plasmas **8**, 423 (2001).
[12] V. V. Gorgadze, L. Friedland, and J. S. Wurtele, Phys. Plasmas **14**, 082317 (2007).
[13] W. Bertsche, J. Fajans, and L. Friedland, Phys. Rev. Lett. **91**, 265003 (2003).
[14] G. B. Andresen, M. D. Ashkezari, M. Baquero-Ruiz *et al.* (ALPHA Collaboration), Phys. Rev. Lett. **106**, 025002 (2011).
[15] C. Amole, M. D. Ashkezari, M. Baquero-Ruiz *et al.* (ALPHA Collaboration), Phys. Plasmas **20**, 043510 (2013).
[16] J. Fajans, E. Gilson, and L. Friedland, Phys. Plasmas **6**, 4497 (1999).
[17] J. Fajans and L. Friedland, Am. J. Phys. **69**, 1096 (2001).
[18] H. Higaki, Y. Abo, K. Ito, H. Okamoto, and K. Gomberoff, in *Non-Neutral Plasma Physics IX*, edited by Y. Soga, A. Sanpei, and H. Himura, AIP Conf. Proc. No. 1668 (AIP, Melville, 2015), p. 050006.
[19] R. Chu, J. S. Wurtele, J. Notte, J. Peurrung, and J. Fajan, Phys. Fluids B **5**, 2378 (1993).
[20] F. Peinetti, F. Peano, G. Coppa, and J. Wurtle, J. Comput. Phys. **218**, 102 (2006).
[21] K. Gomberoff, J. Wurtle, A. Friedman, D. P. Grote, and J.-L. Vay, J. Comput. Phys. **225**, 1736 (2007).
[22] K. Gomberoff, J. Fajans, J. Wurtle, A. Friedman, D. P. Grote, R. H. Cohen, and J.-L. Vay, Phys. Plasmas **14**, 052107 (2007).
[23] K. Gomberoff, J. Fajans, A. Friedman, D. P. Grote, J.-L. Vay, and J. Wurtle, Phys. Plasmas **14**, 102111 (2007).
[24] H. Higaki, K. Fukata, K. Ito, H. Okamoto, and K. Gomberoff, Phys. Rev. E **81**, 016401 (2010).
[25] K. Moriya, K. Fukushima, K. Ito, T. Okano, H. Okamoto, S. L. Sheehy, D. J. Kelliher, S. Machida, and C. R. Prior, Phys. Rev. ST Accel. Beams **18**, 034001 (2015).